Test Structures for the Wafer Mapping and Correlation of the Properties of Electroplated Ferromagnetic Alloy Films

Test Structures for the Wafer Mapping and Correlation of the Properties of Electroplated Ferromagnetic Alloy Films

Evgeny Sirotkin, Stewart Smith, *Senior Member, IEEE,* Ross Walker, Jonathan G. Terry, *Senior Member, IEEE,* and Anthony J. Walton, *Senior Member, IEEE*

***Abstract*—This paper presents a method of electrically determining the permeability of patterned, electroplated ferromagnetic alloys and brings together the simultaneous wafer mapping of relative permeability, electrical resistivity and mechanical strain of these electrodeposited films, as well as the layer thickness and alloy composition. The wafer mapping of all these properties is implemented using a set of simple, automated electrical and optical techniques that facilitate the quantification of the spatial correlation between different parameters. This enables the uniformity of conductive ferromagnetic films to be analysed and supports the optimization of the physical properties of these materials as well as the processes used to deposit them.**

***Index Terms*—Wafer mapping, electroplated ferro-magnetic films, integrated magnetic technologies, automated test development, characterisation.**

I. Introduction

ELECTROPLATING is considered today as perhaps the most effective manufacturing process for the production of ferromagnetic thin films with thicknesses ranging from hundreds of nanometres up to tens of micrometres. Ferromagnetic films are essential elements in a number of different applications involving heterogeneous integration. For example, integrated passive magnetic components including inductors and transformers are key to the development of on-chip smart power systems such as DC-DC converters [1]–[3]. There are many applications for magnetic materials in the field of micro-electromechanical systems (MEMS) [4], [5] including magnetically actuated switches and relays [6], [7], energy harvesting systems [8] and magnetic field sensors like fluxgates [9]. The basic physical properties of importance for these device applications include the magnetic permeability, electrical resistivity and mechanical residual stress. As far as the authors are aware, the use of test structures capable of the routine, wafer-level measurement of permeability using standard electrical probing has not been previously reported and hence, the spatial variability of permeability has not been wafer mapped. The ability to perform this measurement with relatively simple electrical measurements provides the opportunity to provide fast feedback on the magnetic performance of electrodeposited materials, which is an essential capability required for process control and verification.

In this work, automated wafer mapping measurements [10]–[16], are reported and used to identify the spatial correlation between high frequency permeability, electrical resistivity, and mechanical residual strain as well as the chemical composition of a nickel-iron alloy film electroplated on the surface of 75 mm diameter silicon wafers. It has been previously reported [17] that NiFe films with $Ni_{79}Fe_{21}$ produce the optimum permeability values, and alloys around this value are commonly referred to as "Permalloy". The ability to extract the permeability of deposited layers on wafer will facilitate the development of magnetic MEMS based technologies.

To make it feasible to routinely determine all the parameters of interest, automated wafer scale measurement and analysis is required in order to:

1) Characterise the spatial distribution of key material parameters across the wafer.
2) Determine the optimal compromise between magnetic, electrical and mechanical properties required for a particular device application.

For example, in the case of micro-inductors, which have been the driver for much of this work, the permeability, resistivity, alloy composition and stress parameters associated with ferromagnetic alloys will define the inductance, resistive core loss and mechanical reliability. This work presents an on-chip test structure based measurement of permeability together with the application of a set of other test structures to allow semi-automated measurement and cross wafer mapping of these and other parameters.

This paper is an extension of [15] presented at the International Conference on Microelectronic Test Structures, and updates and expands a number of elements in the original paper. It presents more comprehensive results along with a more detailed explanation of the on-chip electrical measurements and associated permeability extraction method. Selected wafer maps and scatter plots of the important parameters are presented to illustrate the correlations between magnetic alloy composition and physical parameters such as resistivity, permeability and mechanical strain.

This work was supported in part by EPSRC through the FS/01/02/10 IeMRC Flagship Project on Smart Microsystems. We would also like to acknowledge the financial support of Texas Instruments.

All data used within this publication can be accessed at: http://dx.doi.org/10.7488/ds/1427

E. Sirotkin, R. Walker, J.G. Terry and A.J. Walton are, or were, with The Institute for Integrated Micro and Nano-Systems, The University of Edinburgh, SMC, Alexander Crum Brown Road, Edinburgh EH9 3FF, UK. R. Walker is now with the School of Engineering and Physical Sciences, Heriot Watt University.

S. Smith is with the Institute for Bioengineering, The University of Edinburgh, SMC, Alexander Crum Brown Road, Edinburgh EH9 3FF (e-mail: Stewart.Smith@ed.ac.uk).

Manuscript received April, 2016, Revised June, 2016

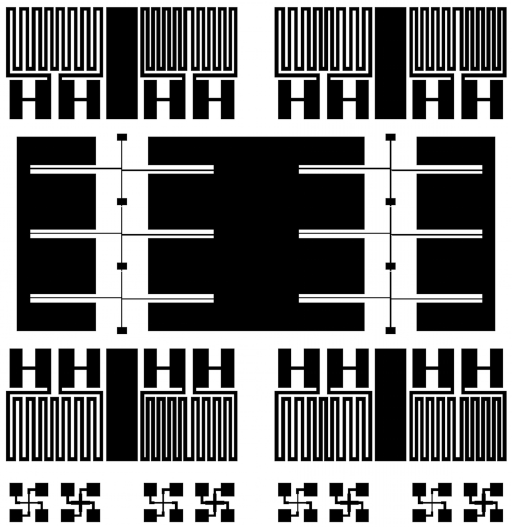

Fig. 1. Layout of 5×5 mm^2 test chip taken from mask for wafer mapping of electroplated ferromagnetic films

II. Test Structure Design and Fabrication

The test chip shown in Fig. 1 was designed to allow a range of physical parameters to be characterised. The design includes MEMS-based strain structures (in the centre) [13], high frequency permeability test structures (top row and second bottom row) and Greek cross electrical test structures (bottom row) [18] which enable a mix of optical (stress) and electrical (DC and RF) measurements on a single wafer. The micro-rotating strain measurement structures have a designed pointer and rotation arm width of 8 μm and three different expansion arm separations of 6, 8 and 10 μm. The designed width of the serpentine resistor sections of the high frequency permeability test structures is 30 μm and there are two different lengths depending on how many ”turns” there are in the serpentine. The Greek cross structures are either 8 μm or 30 μm wide.

The fabrication of the nickel-iron alloy test structures uses bottom up electroplating through a thick photoresist mould patterned using UV lithography on a Karl Süss MA-8 mask aligner. All samples were fabricated on 75 mm (3”) silicon wafers insulated with PECVD silicon oxide, this was used in preference to thermal SiO_2 to allow better results when releasing the MEMS test structures. A 150 nm nickel seed layer has been used to enable plating of the NiFe structures. The nickel seed is preferred to the more typical copper seed layer as the latter would demonstrate a significantly higher conductivity [3] which would greatly affect the results of the skin depth measurements and the extracted data. Further details of the fabrication process can be found in [15], including the HF dry vapour etch process used to release the suspended MEMS structure by removing the sacrificial oxide layer under the pointer and expansion arms. Fig. 2 shows examples of strain structures before and after release. The anticlockwise rotation of the pointer arm in this case shows that there was tensile intrinsic stress in the film before release causing the expansion arms to contract. The level of rotation gives a quantifiable value of the strain (expansion/contraction)

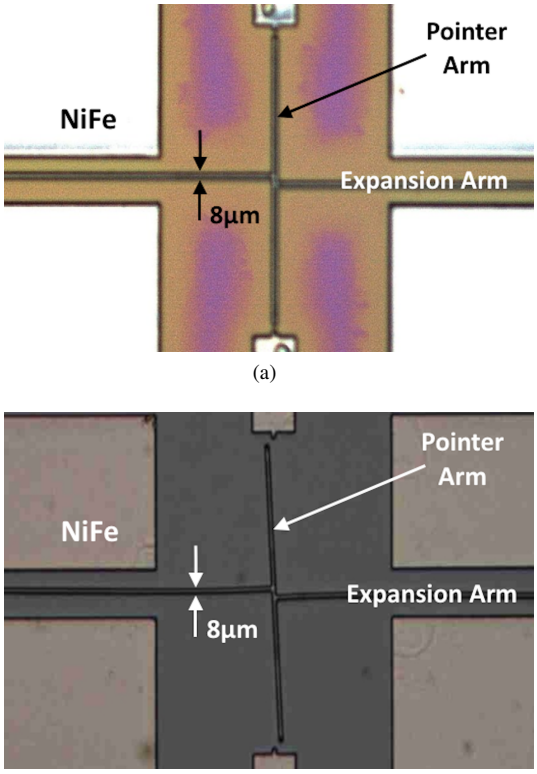

Fig. 2. Strain structures with the expansion arms under tensile stress; (a) unreleased test structure, and (b) released test structure

of the thin film and this information, together with Young’s modulus measured on the structure’s anchor points using a nanoindenter, can be used to extract the stress for each location and wafer map it as detailed in [16].

III. Measurements

Automated test routines for measuring the test structures have been implemented using NI LabVIEW programming with a Karl Suss PA200 semi-automated wafer prober with a digital camera for DC and optical measurements, and a Cascade Summit 12000 probe station for RF measurements. DC resistance measurements are performed using a combination of a HP4142 DC Modular Source/Monitor and an Agilent 3458A Digital Multimeter, while RF (permeability) measurements are made using an Agilent E4991A Impedance/Material Analyzer (1 MHz–3 GHz). The optical measurements of MEMS strain test structures are analysed using custom image processing software [11]. The resulting wafer maps of the extracted physical properties were processed and generated using custom Matlab modules.

The sheet resistance of the NiFe film is measured using the Greek cross structures using a standard test method [10], [18] with a force current of 10 mA. The DC resistances of the 8 and 9 turn serpentine NiFe resistors (see Fig. 3) are measured using a Kelvin connection where the outer pads are used to force a current of 10 mA and the inner pads are used to sense the resulting voltage. In each measurement the current is passed in both the forward and reverse direction, and the calculated resistance values are averaged.

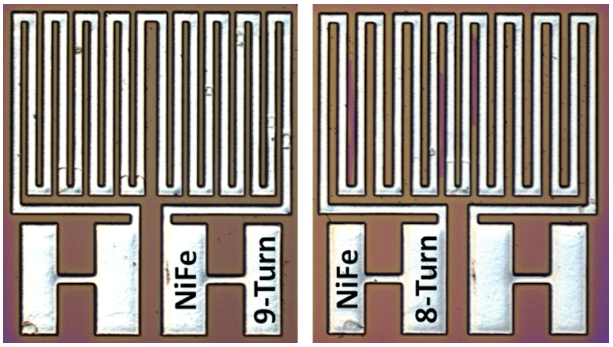

Fig. 3. Serpentine permeability test structures with different numbers of turns

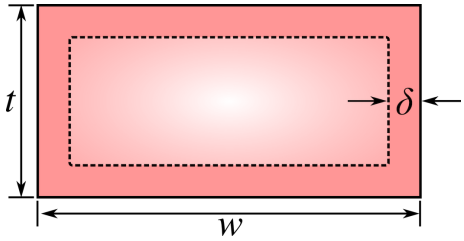

Fig. 4. Schematic diagram showing the geometry represented by the simplified model of skin depth

The high frequency permeability measurements made using the serpentine structures are based on skin depth analysis extracted from RF resistance measured using an impedance meter with an applied AC excitation amplitude of 100 mV and no DC component. The advantages of this approach are that it measures the magnetic properties in the skin depth and enables the magnetic uniformity over wafer to be determined by spatially extracting the permeability at the frequency of interest. It uses an RF electrical measurement without the requirement for an external electromagnet to produce a magnetic field. This makes it possible to perform measurements using standard, RF electrical characterisation equipment. The DC resistance (R_{DC}), the designed width (w) and the measured thickness (t) of the resistor were used to determine DC resistivity (ρ).

$$\rho = \frac{R_{DC} w t}{l} \tag{1}$$

The effective length of the serpentine track (l), was determined based upon a standard method used to calculate the designed resistance of a track given the sheet resistance R_s of the layer, where the resistance of each corner square is $0.56R_s$ [19]. The effective length of the track is simply the number of squares multiplied by the track width (w). The RF resistance (i.e., the real part of the characteristic impedance) at a given frequency (R_{RF}), along with the effective length (l) was used to determine the skin-depth cross-sectional area (A_δ) of the conducting track.

$$A_\delta = \frac{\rho l}{R_{RF}} \tag{2}$$

The skin depth (δ) can then be determined from A_δ and the geometry of the resistor. This calculation uses a simplified model for the skin depth area as illustrated in 4 and expressed mathematically as:

$$A_\delta = 2w\delta + 2t\delta - 4\delta^2 \tag{3}$$

This geometric approximation of skin depth area has been well documented [20]. Clearly, more complex analytical models [21] could be adapted to calculate the skin depth in the permalloy test structure. Equation (4) relates the effective resistance at high frequency (R_{RF}) to the material conductivity (σ); the distribution of the electric field acting through the conductor (E_z) across the rectangular cross section and the cross-sectional width (w) and thickness (t). However, it should be noted that the accuracy of the geometric approximation of skin effect, used in this paper, improves as frequency is increased [22].

$$R_{RF} = \frac{\int_0^t \int_{-w/2}^{w/2} |E_z(x,y)|^2 \, dx \, dy}{\sigma \left| \int_0^t \int_{-w/2}^{w/2} E_z(x,y) \, dx \, dy \right|^2} \tag{4}$$

Solving (3) for δ using the standard quadratic solution gives:

$$\delta = \frac{(2w + 2t) - \sqrt{(-2w - 2t)^2 - 16A_\delta}}{8} \tag{5}$$

Note that the other root gives a non-physical result for δ which is greater than the measured thickness of the electroplated film, and can therefore be disregarded. Finally, the relative permeability (μ_r) can be calculated as follows:

$$\mu_r = \frac{2\rho}{\omega \mu_0 \delta^2} \tag{6}$$

where ω ($2\pi f$) is the angular frequency of the RF signal and μ_0 is the permeability of free space ($4\pi \times 10^{-7}$ H m^{-1}).

IV. Results

Prior to RF measurements, hysteresis BH-loop measurements were performed on unpatterned, 5 μm thick $Ni_{75}Fe_{25}$ films using dedicated Shb Instruments equipment comprising of a 10 Hz oscillating electromagnet and pick-up coils. Fig. 5 presents a set of in-plane hysteresis loops from four separate measurements with the sample rotated by 90°between each. The results show a small coercive field (H_c) of 0.8-1.2 Oe (63.7-95.9 A m^{-1}), a low saturation field (H_s) around 9.0-10.0 Oe (716.2-795.8 A m^{-1}) and low remanent magnetization (<35-40 %). This demonstrates the very soft magnetic behaviour of these films, which is required for low-amplitude RF measurements with no bias. It can be hard to saturate or demagnetise hard magnetic materials. The measurement method used here assumes that the magnetisation within the material follows the magnetic field induced by the electrical current during RF probe measurements.

Fig. 6 shows measured values of resistance, and the extracted values of skin depth and permeability as a function of frequency for a range of NiFe compositions (Fe content 27-35 %). As expected the measured resistance increases with frequency, as the current flow becomes constrained within the skin depth which reduces in thickness as the frequency increases. Fig. 6(b) shows the skin depth as a function of

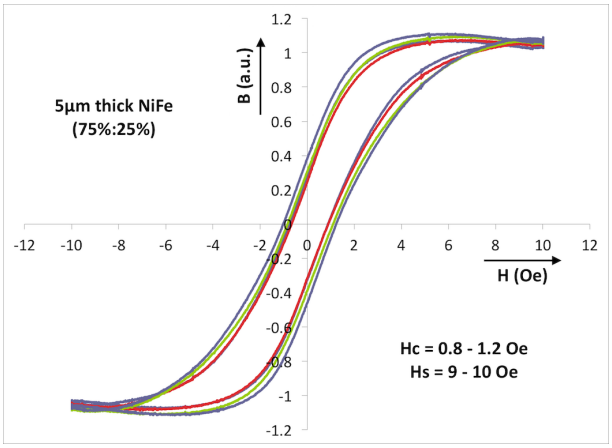

Fig. 5. Hysteresis (BH-loop) measured for a 5 µm thick NiFe films to confirm soft magnetic behavior.

frequency calculated using (5) assuming the simple model described by (3). Clearly if the skin depth δ is greater than or equal to half the thickness of the film the model is invalid and in these cases the calculated value for has no physical meaning. For the measurements associated with Fig. 6 the film thickness of the NiFe alloy is between 15 µm and 19 µm and so we define the maximum valid skin depth δ to be 7 µm. This value of δ is exceeded for results below 10-15 MHz and this in turn identifies the frequency below which the assumptions in the model are no longer valid. Consequently for the results in Fig. 6(b) and (c) we assume that only calculations of skin depth and permeability for frequencies of 15 MHz and above are valid. Fig. 6(b) shows that as expected the skin depth extracted from the resistance measurements reduces as the frequency increases. The associated permeability extracted using the model in (6) is presented in Fig. (c). The results show the permeability decreases as the iron content is increased and that it slowly increases with frequencies above 20 MHz. From equation (5) it can be observed that the permeability depends on two variables: frequency ($\omega = 2\pi f$) and δ. When the frequency increases, the skin depth reduces as shown in Fig. (b). However, the skin depth is squared and therefore, is seen to have a stronger effect on the trend (i.e. the calculated permeability is increasing as the result of the reduction in the calculated skin depth). It should also be noted that apparent discontinuities visible in the graphs are due to range switching in the impedance analyser.

The uniformity of the composition and thickness of the electroplated NiFe was wafer mapped using a Thermo-Scientific X-Ray Fluorescence (XRF) tool, and these results are presented in Fig. 7 along with results of optical measurement of the pointer arm rotation from the MEMS test structures and the sheet resistance results from 8 µm and 30 µm wide Greek cross test structures. The alloy thickness across the wafer was also confirmed at certain points on the wafer using a DekTak surface profiler. The wafer maps of NiFe composition and thickness show different spatial variation patterns. The thickness shows a bull's eye variation with the thinnest material in the centre of the wafer, while the compositional mapping indicates the lowest Fe content at the top right hand side of

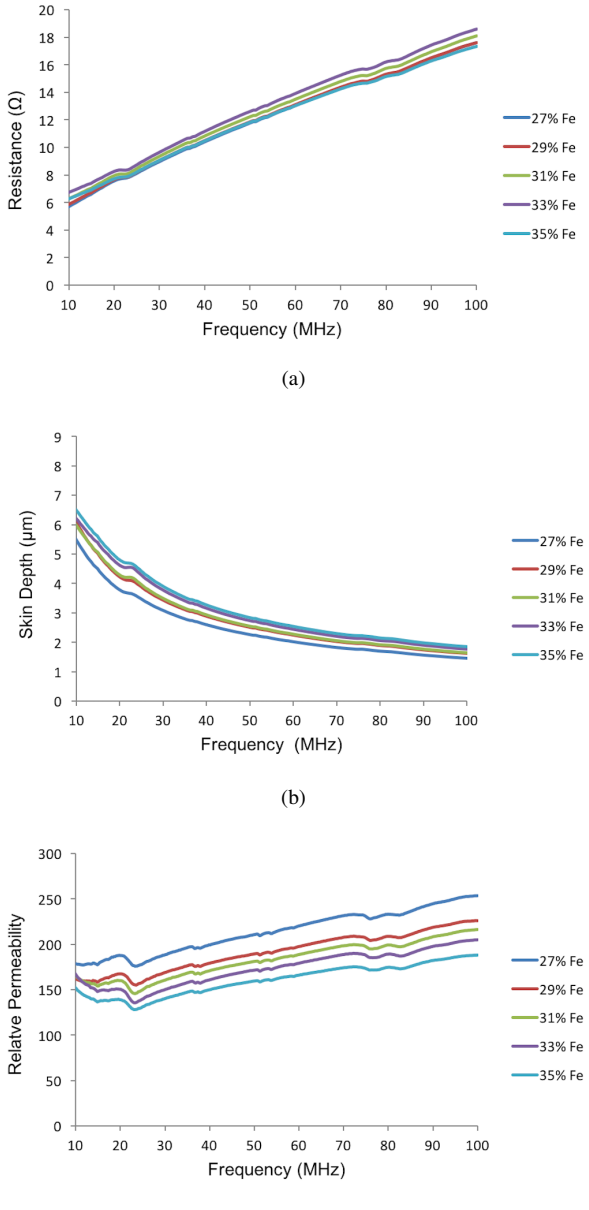

Fig. 6. The effect of iron content in NiFe films ranging between 27% and 35% on the RF resistance (a), skin depth (b), and relative permeability (c) as a function of frequency.

the wafer and the highest values at the bottom left hand side. The sheet resistance results suggest a combination of effects of composition and thickness so that the bull's eye pattern is shifted towards the area of highest Fe content. The measured sheet resistance is higher for the narrower structures suggesting there is a pattern dependent effect on the effective thickness of the material. The 30 µm wide Greek cross structures are more representative of the dimensions of the serpentine resistor structures. The rotation angle indicates the level of strain in the released expansion arms in the structure. This is an indication of the level of intrinsic stress in the film before release. As has been previously reported the level of tensile stress in NiFe films is correlated with the %Fe content. Lower rotations, indicating less stress, are observed where the Fe content is

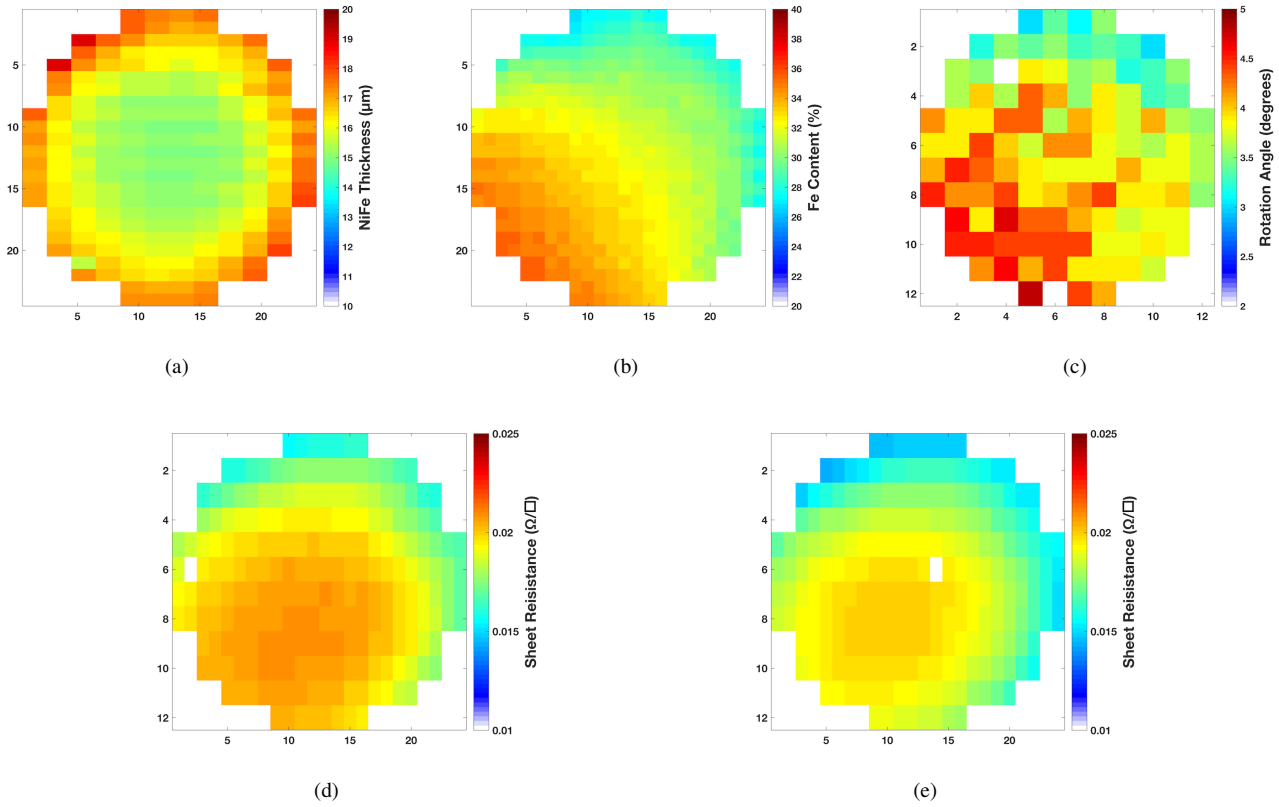

Fig. 7. Wafer maps of (a) electroplated NiFe alloy thickness, (b) alloy composition (%Fe content), (c) MEMS test structure pointer arm rotation, and sheet resistance extracted from (d) 8 µm and (e) 30 µm wide Greek cross structures,

lower. This is a positive result as the target composition ($Ni_{79}Fe_{21}$) for optimum permeability is a lower Fe content than in the films measured here, as in [17].

Fig. 8 shows wafer maps of DC resistance and the derived resistivity for the 8-turn serpentine structures. Similar results from the 9-turn structures can be seen in [15]. Inspection of Fig. 7 and Fig. 8 indicates that the DC resistance wafer map is affected by both the film thickness and composition with the stronger correlation being with the thickness. The film resistivity, which is a material parameter independent of the film thickness, appears to be more strongly correlated with film composition. Fig. 9 shows wafer maps of RF resistance at three different frequencies, and these are also well correlated with thickness up to 100 MHz. Fig. 10 and Fig. 11 show wafer maps of skin depth and permeability respectively, at the same three frequencies. It is apparent that these magnetic properties are most strongly correlated with the %Fe content.

The wafer maps presented above clearly identify the variation of parameters across the wafers, and this can be used to identify the root causes (in this case the circulation of the electrolyte). Even with the spatial non-uniformity displayed in the wafer maps the data can be used to calculate the correlation coefficients between parameters as the measurement locations are known. Table I shows correlation coefficients between the NiFe thickness and the DC resistance, resistivity, and RF resistances. Table II shows correlation coefficients between the NiFe composition and the resistivity, skin depth, and

TABLE I
CORRELATION COEFFICIENTS WITH NIFE THICKNESS

Parameter	Correlation Coefficient	
	8-turn	9-turn
DC Resistance	−0.83	−0.85
Resistivity	−0.41	−0.4
Resistance at 15 MHz	−0.89	−0.9
Resistance at 20 MHz	−0.92	−0.88
Resistance at 100 MHz	−0.87	−0.75

permeability. The data used to prepare the wafer maps can also be presented as correlation scatter plots and Fig. 12 shows plots of relative permeability against %Fe content at 100MHz. It should be noted that such plots do not convey the spatial information of the wafer maps.

In summary it is not surprising these results confirm that the measured permeability depends upon the Ni-Fe ratio and not the layer thickness of the material. This is very important for the design of microinductors with a magnetic alloy core, as the permeability value directly influences the inductance.

V. DISCUSSION AND CONCLUSIONS

The ability to comprehensively and rapidly characterise patterned electroplated magnetic films such as NiFe is an essential requirement when integrating magnetic materials into miniaturised magnetic components and MEMS devices.

TABLE II
CORRELATION COEFFICIENTS WITH COMPOSITION (%FE)

Parameter	Correlation Coefficient	
	8-turn	9-turn
Resistivity	0.90	0.90
Skin depth at 15 MHz	0.88	0.93
Skin depth at 20 MHz	0.92	0.95
Skin depth at 100 MHz	0.91	0.93
Permeability at 15 MHz	−0.78	−0.87
Permeability at 20 MHz	−0.87	−0.87
Permeability at 100 MHz	−0.92	−0.93

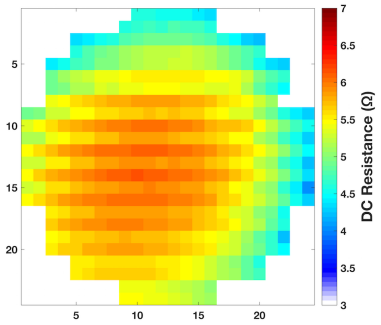

(a) DC resistance

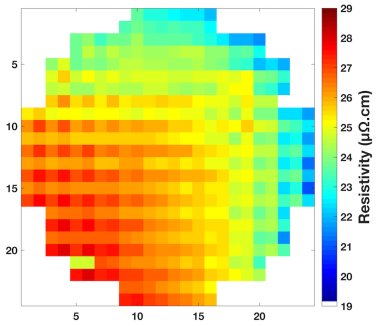

(b) Resistivity

Fig. 8. Wafer maps of DC resistance measurements and estimated resistivity for 8-turn serpentines

Important measurement parameters for such materials includes the spatial characterisation of stress/strain [13], resistance [10], [18], alloy composition [14] and Young's modulus [16] and on-chip measurements of these parameters for wafer mapping have all been previously reported in the literature. The missing element that has not been available as a simple on-chip measurement has been the ability to spatially determine the permeability of magnetic materials electroplated on silicon wafers. The determination of this important parameter has required unpatterned wafers to be diced to create the required samples which are then measured using equipment such as a BH-loop test system. Unfortunately, this procedure is both time-consuming and destructive, and does not support the rapid development of processes to integrate new alloys and evaluate new designs. This paper has addressed this limitation by reporting electrical test structures that enable on-wafer spatial characterisation of permeability. The proposed test structure and its measurement involves the quantification of permeability based on the skin depth effect in resistive structures measured at high frequencies, and for the first time enables permeability to be mapped across a wafer. In contrast with more standard magnetic measurements a key advantage of the proposed method is that the permeability can be extracted from wafer level measurements using standard electrical test equipment. This ability to wafer map permeability completes the capability to wafer map all the key parameters required to characterise patterned electroplated magnetic alloys.

With this capability the paper presents the design and implementation of a test chip for the comprehensive characterisation of on-wafer electroplated ferromagnetic materials. The test chip includes a combination of optically measured micromechanical structures to wafer map the intrinsic stress in electrodeposited films, structures for Young's modulus measurements (nanoindentation), XRF measurements for wafer mapping alloy composition as well as electrical structures for the characterisation of resistance and permeability. The ability to simultaneously wafer map all these parameters supports process development and control enabling properties to be correlated and relationships identified.

For example, the presented measurements demonstrate the correlation between NiFe alloy composition and parameters such as resistivity, permeability and layer stress. As expected, a composition which is closer to the optimum target of 79% nickel and 21% iron, gives a higher value of permeability. The strain indicator structure results show that the lower iron concentration gives a lower level of intrinsic stress, which is a positive finding, but these areas of the wafer also show a lower resistivity for the NiFe material. Low resistance for ferromagnetic cores is undesirable due to increased eddy current losses as described in [3]. The test structures and measurements described in this paper enable rapid process optimisation and development and can easily be applied to other ferromagnetic alloys.

REFERENCES

[1] C. Ó. Mathúna, N. Wang, S. Kulkarni, and S. Roy, "Review of Integrated Magnetics for Power Supply on Chip (PwrSoC)," *Power Electronics*, vol. 27, no. 11, pp. 4799–4816, 2012.

[2] R. Meere, T. O'Donnell, N. Wang, N. Achotte, S. Kulkarni, and S. C. O'Mathuna, "Size and Performance Tradeoffs in Micro-Inductors for High Frequency DC-DC Conversion," *IEEE Transactions on Magnetics*, vol. 45, no. 10, pp. 4234–4237, 2009.

[3] R. Walker, E. Sirotkin, J. Terry, S. Smith, M. Desmulliez, and A. J. Walton, "Effect of seed layers on the performance of planar spiral microinductors," in *2014 International Conference on Microelectronic Test Structures (ICMTS)*, Jan. 2014, pp. 135–140.

[4] N. V. Myung, D. Y. Park, B. Y. Yoo, and P. T. A. Sumodjo, "Development of electroplated magnetic materials for MEMS," *Journal of Magnetism and Magnetic Materials*, vol. 265, no. 2, pp. 189–198, Sep. 2003.

[5] D. Niarchos, "Magnetic MEMS: key issues and some applications," *Sensors & Actuators: A. Physical*, vol. 109, no. 1-2, pp. 166–173, Dec. 2003.

[6] G. Schiavone, S. Smith, J. Murray, J. Terry, M. Desmulliez, and A. J. Walton, "Micromechanical test structures for the characterisation of electroplated NiFe cantilevers and their viability for use in MEMS switching devices," in *2013 IEEE International Conference on Microelectronic Test Structures (ICMTS)*, Jan. 2013, pp. 13–18.

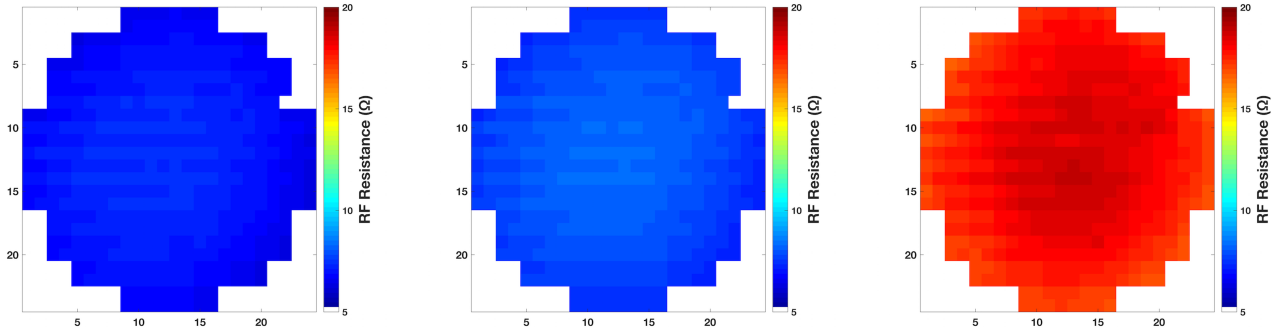

(a) RF Resistance 15 MHz (b) RF Resistance 20 MHz (c) RF Resistance 100 MHz

Fig. 9. Wafer maps of RF resistance measurements for 8-turn serpentines at three different frequencies

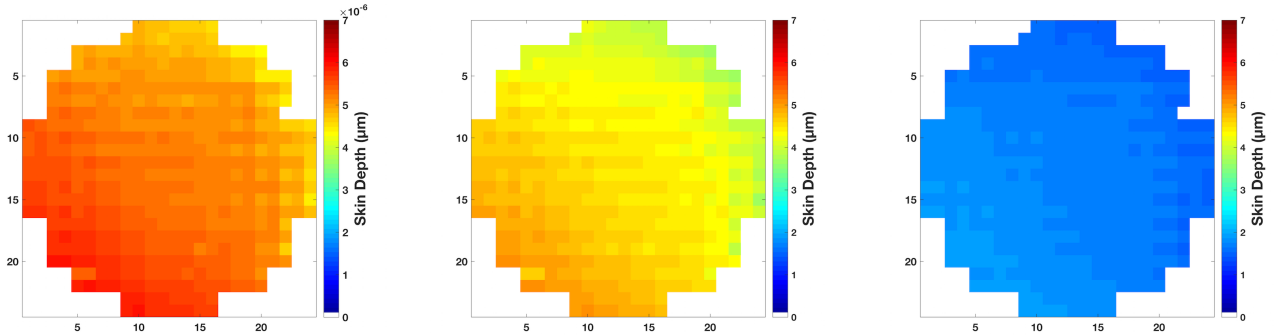

(a) Skin depth 15 MHz (b) Skin depth 20 MHz (c) Skin depth 100 MHz

Fig. 10. Wafer maps of calculated skin depths for 8-turn serpentines at three different frequencies

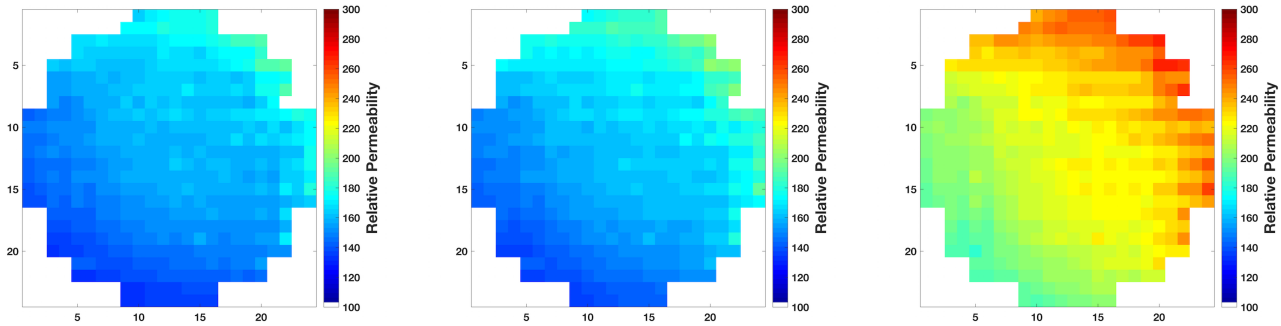

(a) Permeability 15 MHz (b) Permeability 20 MHz (c) Permeability 100 MHz (8 turn)

Fig. 11. Wafer maps of calculated permeability for 8-turn serpentines at three different frequencies

[7] G. Schiavone, M. Desmulliez, and A. Walton, "Integrated Magnetic MEMS Relays: Status of the Technology," *Micromachines*, vol. 5, no. 3, pp. 622–653, Aug. 2014.

[8] M. Han, Q. Yuan, X. Sun, and H. Zhang, "Design and Fabrication of Integrated Magnetic MEMS Energy Harvester for Low Frequency Applications," *Journal Of Microelectromechanical Systems*, vol. 23, no. 1, pp. 204–212, 2014.

[9] O. Zorlu, P. Kejik, and R. S. Popovic, "An orthogonal fluxgate-type magnetic microsensor with electroplated Permalloy core," *Sensors & Actuators: A. Physical*, vol. 135, no. 1, pp. 43–49, Mar. 2007.

[10] A. J. Walton and S. Smith, "A Review of Test Structures for Characterising Microelectronic and MEMS Technology," *Advances in Science and Technology*, vol. 54, pp. 356–365, 2008.

[11] S. Smith, N. Brockie, J. Murray, G. Schiavone, C. Wilson, A. Horsfall, J. Terry, J. T. M. Stevenson, A. Mount, and A. J. Walton, "Fabrication and Measurement of Test Structures to Monitor Stress in SU-8 Films," *Semiconductor Manufacturing, IEEE Transactions on*, vol. 25, no. 3, pp. 346–354, 2012.

[12] J. Murray, S. Smith, G. Schiavone, J. Terry, A. Mount, and A. J. Walton, "Correlation of optical and electrical test structures for characterisation of copper self-annealing," in *Microelectronic Test Structures (ICMTS), 2012 IEEE International Conference on*, 2012, pp. 152–158.

[13] S. Smith, N. Brockie, J. Terry, N. Wang, A. Horsfall, and A. J. Walton, "Application of a Micromechanical Test Structure to the Measurement of Stress in an Electroplated Permalloy Film," in *2009 IEEE International Conference on Microelectronic Test Structures (ICMTS)*, Jan. 2009, pp.

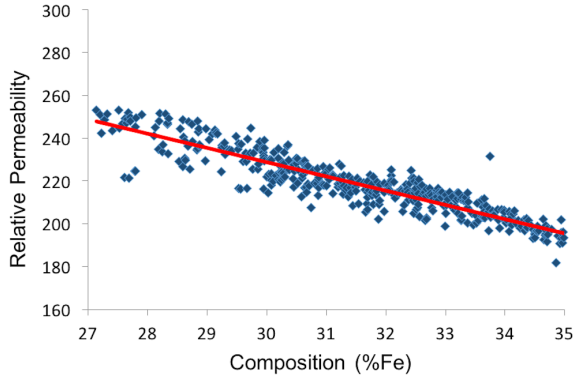

Fig. 12. Correlation scatter plot of relative permeability versus %ge Fe content measured at 100MHz for 8 turn serpentines

75–80.
[14] J. Murray, G. Schiavone, S. Smith, J. Terry, A. Mount, and A. J. Walton, "Characterisation of electroplated NiFe films using test structures and wafer mapped measurements," in *2011 International Conference on Microelectronic Test Structures (ICMTS)*, Apr. 2011, pp. 63–68.
[15] E. Sirotkin, S. Smith, R. Walker, J. Terry, and A. J. Walton, "Test structures for the wafer mapping and correlation of electrical, mechanical and high frequency magnetic properties of electroplated ferromagnetic alloy films," *2015 International Conference on Microelectronic Test Structures (ICMTS)*, pp. 182–187, Mar. 2015.
[16] G. Schiavone, M. Desmulliez, S. Smith, J. Murray, E. Sirotkin, J. Terry, A. Mount, and A. Walton, "Quantitative wafer mapping of residual stress in electroplated NiFe films using independent strain and Young's modulus measurements," in *IEEE International Conference on Microelectronic Test Structures (ICMTS)*, Jan. 2012, pp. 105–110.
[17] H. D. Arnold and G. W. Elmen, "Permalloy, an alloy of remarkable magnetic properties," *Journal of the Franklin Institute*, vol. 195, no. 5, pp. 621–632, May 1923.
[18] M. Buehler and W. Thurber, "An experimental study of various cross sheet resistor test structures," *Journal of the Electrochemical Society*, vol. 125, p. 645, 1978.
[19] R. C. Jaeger, *Introduction to Microelectronic Fabrication*, ser. Volume 5 of Modular Series on Solid State Devices, G. W. Neudeck and R. F. Pierret, Eds. Pearson, 2013.
[20] K. L. Kaiser, *Electromagnetic Compatibility Handbook*. CRC Press, Sep. 2004.
[21] R. Faraji-Dana and Y. Chow, "Edge condition of the field and AC resistance of a rectangular strip conductor," *IEE Proceedings H - Microwaves, Antennas and Propagation*, vol. 137, no. 2, pp. 133–140, Apr. 1990.
[22] M. Matsuki and A. Matsushima, "Improved Numerical Method for Computing Internal Impedance of a Rectangular Conductor and Discussions of its High Frequency Behavior," *Progress In Electromagnetics Research M*, vol. 23, pp. 139–152, 2012.

Evgeny Sirotkin graduated from Saratov State University, Russia in 2006 with specialist diploma in "Microelectronics and Semiconductor Devices" while he was also working at UniqueICs LLC during the last 2 years. In 2010 he graduated with a PhD in Physics from the University of Exeter working on magnetic materials. Since then, Evgeny has worked on industrial projects at leading research institutions including CEMPS (University of Exeter) and SMC (The University of Edinburgh) and at innovative microelectronic design centres including ARM. His professional interests include: SoC/ASIC design and implementation, electronics prototyping, test automation, microelectronic test structures for wafer mapping and yield analysis and MEMS/microsystems.

Stewart Smith (SM'12) received the B.Eng.(hons) degree in electronics and electrical engineering in 1997 and the Ph.D. degree in 2003 from the University of Edinburgh, Scotland, UK. He is currently a lecturer in the School of Engineering at the University of Edinburgh and a member of the Research Institute for Bioengineering. Stewart is a member of the technical committee for the IEEE International Conference on Microelectronic Test Structures and an officer of the Scottish Chapter of the IEEE Electron Devices Society. His current research interests include the design and fabrication of bioelectronic and biomedical microsystems, microfluidics and biosensors, and development of test structures for MEMS and microsystems processes.

Ross Walker received the M.Eng. degree in in 2011 from Heriot-Watt University and the Ph.D. degree in 2016 from the University of Edinburgh, Scotland, UK. He is currently a Research Associate in the Institute of Mechanical Process and Energy Engineering at Heriot-Watt University. His current research interests include the design and fabrication of microinductors, microfabrication, microassembly, magnetics, and development of test structures for MEMS processes.

Jonathan G. Terry (SM'08) received the B.Eng. degree in electronics engineering, the M.Sc. degree in microelectronic material and device technology, and the Ph.D. degree in solid-state electronics from the University of Manchester Institute of Science and Technology, Manchester, U.K. He joined the Institute for Integrated Micro and Nanosystems, University of Edinburgh, Edinburgh, U.K., in 1999, as a Research Fellow. He is currently a Chancellor's Fellow and Lecturer with the University of Edinburgh, where his main area of interest is in the development of More-than-Moore technologies, and the integration of novel fabrication processes and materials with foundry CMOS to create smart microsystems. He is a Treasurer of the Scottish Chapter of the IEEE Electron Devices Society and Region 8 (U.K., Africa, and Middle East) Editor of the EDS Newsletter.

Anthony J. Walton (SM'88) is currently Professor of Microelectronic Manufacturing with the School of Engineering, University of Edinburgh, Edinburgh, U.K. Over the past 25 years, he has been actively involved with the semiconductor industry in a number of areas associated with silicon processing that includes both integrated circuit technology and microsystems. In particular, he has been intimately involved in the development of technologies and their integration with CMOS. He played a key role in setting up the Scottish Microelectronics Centre, Edinburgh, which is a purpose-built facility for research and development and commercialization. He is a Fellow of the Royal Society (Edinburgh) and has served as the Chairman for a number of conferences, including the European Solid-State Devices Research Conference in 1994 and 2008, and ICMTS in 1989 and 2008.